Plasmonic gold nanoparticles for detection of fungi and human cutaneous fungal infections

Citation: Sojinrin, Tobiloba; Conde, João; Liu, Kangze; Curtin, James; Byrne, Hugh J.; Cui, Daxiang and Tian, Furong. "Plasmonic Gold Nanoparticles for Detection of Fungi and Human Cutaneous Fungal Infections." Analytical and Bioanalytical Chemistry 409, 19 (June 2017): 4647–4658 © 2017 Springer-Verlag Berlin Heidelberg

As Published: http://dx.doi.org/10.1007/s00216-017-0414-7

Publisher: Springer-Verlag

Persistent URL: http://hdl.handle.net/1721.1/110585

Version: Author's final manuscript: final author's manuscript post peer review, without publisher's formatting or copy editing

Plasmonic gold nanoparticles for detection of fungi and human cutaneous fungal infections

Tobiloba Sojinrin[1], João Conde[2,3,*], Kangze Liu[1], James Curtin[1], Hugh J Byrne[4], Daxiang Cui[5], Furong Tian[1,*]

[1] Environmental Sustainability and Health Institute, School of Food Science and Environmental Health, College of Sciences and Health, Dublin Institute of Technology, Cathal Brugha Street, Dublin 1, Ireland

[2] Massachusetts Institute of Technology, Institute for Medical Engineering and Science, Harvard-MIT Division for Health Sciences and Technology, 77 Massachusetts Avenue, Cambridge, Massachusetts 02139, USA

[3] School of Engineering and Materials Science, Queen Mary University of London, Mile End Road, London E1 4NS, United Kingdom

[4] FOCAS Research Institute, Dublin Institute of Technology, Camden Row, Dublin 8, Ireland

[5] Institute of Nano Biomedicine and Engineering, Key Lab for Thin Film and Microfabrication Technology of Education Ministry, Department of Instrument Science and Engineering, National Center for Translational Medicine, Shanghai Jiao tong university 800 Dongchuan road, Shanghai 200240, China

* Corresponding authors:
João Conde: jdconde@mit.edu
Furong Tian: furong.tian@dit.ie

ABSTRACT

Fungi, which are common in the environment, can cause a multitude of diseases. Warm, humid conditions allow fungi to grow and infect humans via the respiratory, digestive and reproductive tracts, genital area and other bodily interfaces. Fungi can be detected directly by microscopy, using the potassium hydroxide (KOH) test, which is the gold standard and most popular method for fungal screening. However, this test requires trained personnel operating specialist equipment, including a fluorescent microscope and culture facilities. As most acutely infected patients seek medical

attention within the first few days of symptoms, the optimal diagnostic test would be rapid and self-diagnostic simplifying and improving the therapeutic outcome. In suspensions of gold nanoparticles, *Aspergillus niger* can cause a colour change from red to blue within 2 minutes, as a result of changes in nanoparticle shape. A similar colour change was observed in the supernatant of samples of human toenails dispersed in water. Scanning electron microscopy, UV/Vis and Raman spectroscopy were employed to monitor the changes in morphology and surface plasmon resonance of the nanoparticles. The correlation of colour change with the fungal infection was analysed using the absorbance ratio at 520nm/620nm. We found a decrease in the ratio when the fungi concentration increased from 1 to 16 CFU/mL, with a detection limit of 10 CFU/mL. The test had an 80% sensitivity and a 95% Specificity value for the diagnosis of Athlete's foot in human patients. This plasmonic gold nanoparticle-based system for detection of fungal infections measures the change in shape of gold nanoparticles and generates coloured solutions with distinct tonality. Our application has the potential to contribute to self-diagnosis and hygiene control in laboratories/hospitals with fewer resources, just using the naked eye.

Keywords Fungi, gold nanoparticles, plasmonic assay, self-diagnostic

INTRODUCTION

Fungi are ubiquitous in nature and can occur as unicellular yeast or filamentous bodies, as well as multicellular moulds [1]. When the climate is mild, moist and changeable with abundant rainfall in summer, the high humidity level allows fungi to grow on the surface of materials, causing human infections such as *onychomycosis* and *Tinea pedis* [2]. People with onychomycosis may experience significant psychosocial problems due to the appearance of the nail, particularly when fingers are infected [3, 4]. Onychomycosis is primarily caused by *Dermatophytes* (mainly *Trichophyton rubrum* and *T. mentagrophytes*) and to a lesser extent by nondermatophyte fungi such as *Acremonium* spp., *Aspergillus* spp., *Fusarium* spp., *Scopulariopsis brevicaulis*, *C. albicans*, and *C. parapsilosis* [5-13]. *Tinea pedis* (Athlete's foot) is another example of disease inflicted by *Aspergillus* fungi in humid weather. This disease may cause foot itching, burning, pain, and can be spread from person to person or by walking on contaminated objects and floors [1]. The genus *Aspergillus* is comprised of several hundred species that are ubiquitous in the environment [3]. The most common fungi are *Aspergillus*

fumigatus, *Aspergillus flavus*, *Aspergillus niger*, and *Aspergillus terreus* [4]. Several non-dematiaceous fungi may also cause fungal melanonychia, including *Trichophyton rubrum*.

Despite their widespread occurrence, little attention has been given to the development of new methods to detect the presence of such fungi [2]. Currently available diagnostic tools for detecting fungal infection include polymerase chain reactions (PCR) and enzymes [14]. However, PCR protocols have their own drawbacks, which limit their widespread application. Unfortunately, false-positive results occur in 5.7%–14.0% of adults and as high as 83% in neonates [5]. On the other hand, the use of PCR to detect fungal DNA is possible in research laboratories, but is not standardized or FDA approved [15]. Notably, the sensitivity of PCR is higher in *in vitro* colonization than in patient infections and may cause false positives [15]. Microbiological cultures of biological fluids and tissue for the detection of an invasive fungal infection require multiple days and occasionally weeks for the identification of a specific fungal pathogen [16, 17]. Serological diagnosis using PCR, antibody, and toxins requires a modern medical infrastructure including expensive equipment, costly materials and well-trained specialists to operate the system [18, 19]. The gold standard procedure for fungal screening is directly by microscopy using a potassium hydroxide (KOH) test [19]. The KOH test is usually conducted on an outpatient basis. Results are usually available while the patient waits or on the next day, if sent to a clinical laboratory [19]. However, it requires fluorescence microscopy, as well as specialised culture conditions, which makes this method time consuming and requires specific training. As most acutely infected patients seek medical attention within the first few days of illness, a cheap, fast and simple test would allow simple home diagnosis and would support identification and intervention in regions with underdeveloped medical systems or access to clinical testing.

Gold nanoparticles have been extensively investigated for cancer diagnosis [20-28]. Recently, an assay has been developed for HIV detection with the naked eye based on gold nanoparticle formulation [29]. The temperature, pH value and salt concentration have been intensively studied to examine their impact on the process of gold nano particle formulation on *Rhizopus oryzae* protein extract [30,31]. Here, we describe the development of a protocol to formulate gold nanoparticles, which react with spore forming fungi e.g. *Aspergillus niger*, *Aspergillus Oryzae* , *Penicillium Chrysogenum* and *Mucor Hiemalis* resulting in changes of gold nanoparticles' (GNPs) shape and therefore colour, detectable with the naked eye [20,32] (see Figure 1). The goal of this study is to

further develop a rapid method for hygiene control based on gold nanoparticles. The development of a fungi detection with the naked eye is imperative, due to the growing evidence of links between microbial contamination and various types of health issues [33]. Samples from 25 humans were investigated and the results were compared between gold nanoparticle method and the existing clinic test, KOH on athlete's foot.

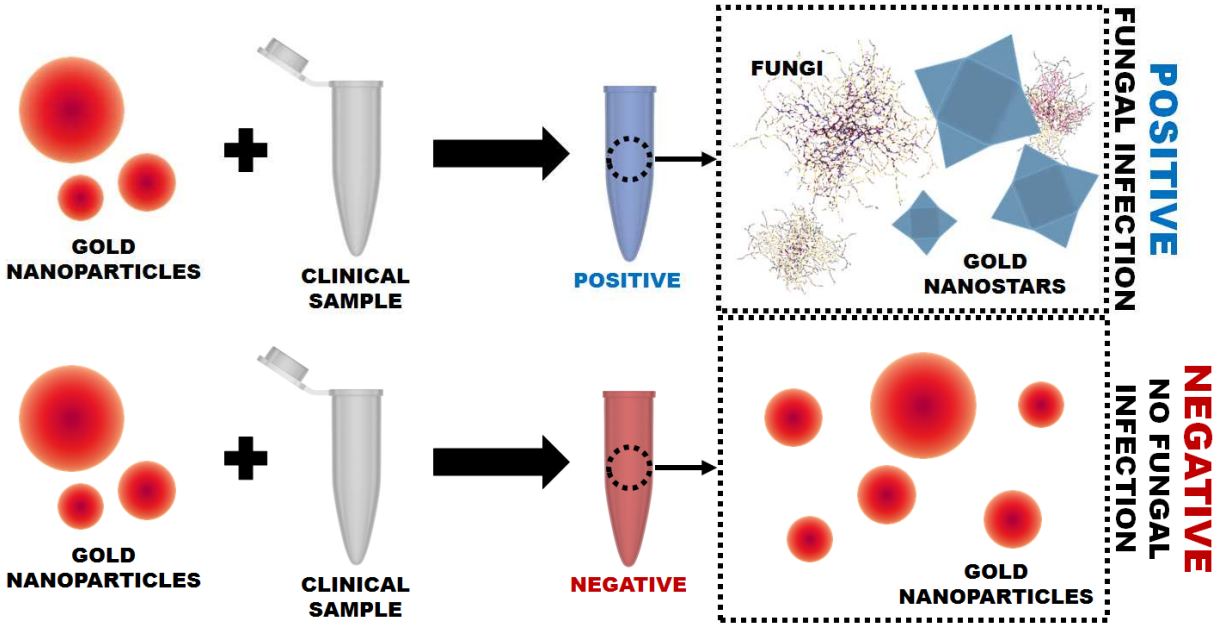

Figure 1. Schematic representation of the Plasmonic Fungi Gold nanoparticle system for self-diagnostic and hygiene control of clinical fungal infection with the naked eye.

MATERIALS AND METHODS

Materials

Hydrogen tetrachloroaurate(III) trihydrate ($HAuCl_4 \cdot 4H_2O$) and Costar Clear Polystyrene 96-Well Plates were purchased from Fisher Chemical. Ascorbic acid, $AgNO_3$, cetyltrimethylammonium bromide (CTAB), 10 nm gold colloid suspensions (6×10^{12}/mL), HEPES buffer and Coomassie Blue solution were purchased from Sigma Aldrich. Ultrapure deionized water (resistivity greater than 18.0 $M.\Omega.cm^{-1}$) was used for all solution preparations and experiments.

Synthesis of Colloidal Gold diagnostic reagent

In order to produce a rapid test, the evolution of gold nano particle formulation was considered. The formulation should be rapid and the colour difference identifiable and distinguishable with the naked eye.

Initially. the GNP formation process was studied in the absence of fungal samples. Stock solutions of 2 mM Chloroauric acid and 0.1 M HEPES buffer (Sigma-Aldrich) in deionized water were prepared. 10 µl of the 2 mM Chloroauric acid stock solutions were added to a 96 well plate and mixed with 2 µl of the HEPES buffer in 88 µl distilled water. The colour of the solution changed from pale yellow to pink (indicating the formation of gold nanoparticles). The stability of the gold diagnostic reagent solution was tested over 6 months at room temperature (20 °C). In addition, different concentrations of $NaNO_3$ in the range 0-200 mM were tested for salt stability of the gold nano particle formation rate in Chloroauric acid and HEPES buffer solution.

GNP formulation was also studied in the presence of fungal cultures and human toenail samples. The pH values of Chloroauric acid and HEPES buffer solution were adjusted by addition of HCl. A range of pH values from 2.5 to 7.5 was employed in the GNP formulation in Chloroauric acid and HEPES buffer solution in the presence of fungi. The rate of GNP formulation was monitored.

Characterisation of Colloidal Gold diagnostic reagent

A Perkin Elmer Lambda 900 UV/VIS/NIR Spectrometer was used to measure the absorbance and to observe the formation and stability of GNPs. A Zetasizer Nano ZS analyser (Malvern Instruments, Worcestershire, UK) was used to measure the hydrodynamic particle size and zeta potentials of the nanoparticles. Six replicates have been measured for each data point.

Preparation of samples of fungal infection for testing

Toenails: All the experiments used in this study complied with current ethical considerations: Approval (SYXK-2007-0025) of the Ethical Committee of *Shanghai Jiao Tong University* (Shanghai, China). In this study, verbal informed consent was provided from participants, clients of nail salons. As some salons may not uphold optimum sanitary conditions, a customer with a fungal infection may unknowingly spread the infection causing a serious hygiene issue to the other customers. This may cause discrimination, embarrassment and damage to a customer's self-esteem. The participants were informed that the study is scientifically relevant and not invasive and their

actions would contribute to developing a cheap, fast and simple test, which will improve population living standards. The participants agreed to join the research test anonymously. The participants and the ethic committees approved this consent procedure.

Ten nail clippings from each of the 25 anonymous volunteers in nail salons of foot spas were carefully collected in sterile Eppendorf tubes at room temperature. The same day, the samples were transferred to the laboratory, for gold nanoparticle method, KOH staining and routine fungal culturing. 1.5 mL of Ultrapure deionized water was added and the Eppendorf tubes were shaken. The supernatants were mixed with Chloroauric acid and HEPES buffer for two mins to observe the results. The nails clippings were left in the Eppendorf tubes for the KOH experiment.

KOH assay for detecting fungal infection in a human sample

1 ml of 10% potassium hydroxide was added to the nail clippings Eppendorf and they were incubated at room temperature for fifteen minutes. The nail clippings were then placed onto a microscope slide. Fungi are transparent and therefore, to make them more visible, 10% lactophenol cotton blue stain was added and the slides were observed under bright field microscopy. A fluorescence microscope was used for fungal detection according to the KOH method.

Fungi culture

Aspergillus niger ATCC 16404, *Aspergillus oryzae* LZB125, *Penicillium Chrysogenum* LZB 141 and *Mucor hiemalis* LZB 136 strains were supplied by Blades Biological Ltd. 100 µl of fungi liquid was spread and incubated in a sterile container for inoculation on Sabouraud dextrose agar (SDA) at 25ºC for 5 days. Fungi were harvested in the sterile ultrapure deionized water and centrifuged at 8,720xg for 10 min. The fungi pellet was washed twice with sterile ultrapure deionized water. The pellet was re-suspended in sterile ultrapure deionized water, at a concentration of 1-100 CFU/mL, The *Aspergillus niger* colonies were counted to obtain an optimal concentration of fungi [34]. The re-suspended fungi in sterile ultrapure deionized water was mixed with 2 mM Chloroauric acid and HEPES buffer which was then dropped onto a silicon wafer and observed under Optical and Scanning Electron Microscopic (SEM).

Bacterial strain culture

In order to ensure the GNP sensing effect is not due to bacterial contamination, three bacteria types,

E. coli ATCC 25922, *Bacillus cereus* NCTC 11145 and *Staphylococcus aureus* NCTC 12493 were used in this study. Strains were selected to facilitate comparison with fungi studies on gold nanoparticles. Bacteria were spread on Tryptic soy agar (TSA, Scharlau Chemie) and incubated overnight at 37 ºC. Bacteria were harvested in sterile Ultrapure deionized water and centrifuged at 8,720x g for 10 min. The cell pellet was washed twice with sterile Ultrapure deionized water, and re-suspended at a concentration of 1-100 CFU/ml. The bacterial density was determined by measuring the absorbance at 550 nm using the McFarland standard (BioMérieux, Marcy-l'Étoile, France).

Morphology observation under light Microscopy

100 µl of *Aspergillus niger*, which had been re-suspended in liquid, was mixed with 200 µl of gold nanoparticle suspension. The mixture was loaded in a 1.5 ml Eppendorf tube and centrifuged at 1000 rpm using Shandon cytospin 3. The mixture was spread onto a glass slide, mounted with mounting medium and covered with a cover slide. The fungal structures with gold nanoparticles were examined using a BX51-P Olympus microscope with 100× objective.

Scanning Electron Microscopy of nanoparticle: fungi

100 µl of *Aspergillus niger*, which had been re-suspended in liquid, was mixed with 2 mM Chloroauric acid (10 µl) and 2 µl HEPES buffer in 88 µl distilled water. The mixture was deposited onto silicon substrates. The samples were air dried immediately by spinning for 30 seconds and 2 minutes on silicon substrates. The samples for gold nanoparticle without *Aspergillus niger* were chosen as a negative control (0 seconds). The sample on the silicon substrate was characterised by Scanning Electron Microscopy using a Hitachi SU6600 FESEM instrument at an acceleration voltage of 25 kV. SEM images were taken using the Secondary Electron detector.

Layout of concentration of fungi and bacteria on 96 well plates

The mixture with 2 mM Chloroauric acid (10 µl) and 2 µl HEPES buffer in 88 µl distilled water was added to the 96 well plate. The wells of the first row were blank, containing 100 µl Ultrapure deionized water. The wells from the second to fifth row were filled with 100 µl fungi suspensions. The concentration of fungi were 0, 1, 2, 4, 6, 8, 10, 12, 14, 16 CFU/ml from left to right in each row. The wells from second to fifth row were replicas for each fungi 96-well plate. Four replicates have been

measured for each data point. A plate layout of four fungi together from top to bottom was comprised of *A.niger* in the second row *A.oryzae* in the third, *P.chrysogenum* in the fourth and the fifth with *M.hiemalis*. The plate layout of three bacterial samples starting from the second row to fourth row were *Escherichia. coli*, *Bacillus cereus* and *Staphylococcus aureus.*

Surface Plasmon resonance analysis of nanoparticle: fungi

A Perkin Elmer Lambda 900 UV/VIS/NIR Spectrometer and Zetasizer Nano ZS analyser (Malvern Instruments, Worcestershire, UK) were used to measure the absorbance, hydrodynamic particle size and zeta potentials of the nanoparticles and to observe the formation and stability of GNPs. The diameter, Zeta Potential and Surface Plasmon Resonance of the colloidal gold diagnostic reagent solutions were measured immediately after the *Aspergillus niger* supernatant liquids were added into the Chloroauric acid and HEPES buffer solution.

Raman spectral analysis to confirm fungal contamination

Raman spectroscopy was performed with a HORIBA Jobin Yvon HR800 spectrometer with 785 nm diode laser as source. Spectral data was collected using a 10× microscope objective over the range 400-1800 cm^{-1} with a 10 sec integration time. The detector used was a 16-bit dynamic range Peltier cooled CCD detector. Mixtures of gold nanoparticles and re-suspended cultured fungi solutions were dropped onto CaF_2 substrates and measured immediately. For comparison, spectra of GNPs alone were recorded.

It has been shown that the spectrum of Mycotoxin can be achieved using GNPs and SERS within a few minutes [35, 36]. In order to confirm fungal infection by Raman spectroscopy, Surface Enhanced Raman of gold nanoparticles incubated with fungi were measured according to the preview methods of gold nanostars for surface-enhanced Raman scattering [35, 36, 37].

Statistical Analysis

Two-tail analysis with Fisher's test was employed to evaluate the prediction given, indicating that the method can successfully predict the outcome. The sensitivity and specificity of the gold nanoparticle test and the gold standard KOH method for fungal infection was employed to compare these two assays.

RESULTS AND DISCUSSION

Physico-chemical characterisation of Gold Nanosphere

In the absence of fungi, the colour of solution changes from pale yellow to pink in 10 mins, consistent with gold nanosphere particle formulation. At, Figure 2A shows a scanning electron microscopy image of pristine 35 nm gold nanospheres, precipitated from suspension after the colour change has stabilised (t=0) (left panel of Figure 2A). UV/visible spectra of nanoparticles present a single peak at a wavelength of 520 nm (left panel of Figure 2B), which is consistent with the Surface Plasmon Resonance (SPR) of spherically shaped gold nanoparticles.

Table 1 presents the key physico-chemical characteristics of nanoparticles used in the first GNP formulation study, as determined by a combination of DLS, zeta potential and UV/visible absorption spectroscopy. In the absence of fungi, the DLS of the GNP solutions indicates a monomodal dispersion with a hydrodynamic diameter of 35.4-38.1 nm and a zeta potential of 25.5-26.3 mV. The stability of the spherical shaped colloidal gold diagnostic reagent solution in individual and batch forms was tested and they were seen to remain stable over 6 months at room temperature (Table1).

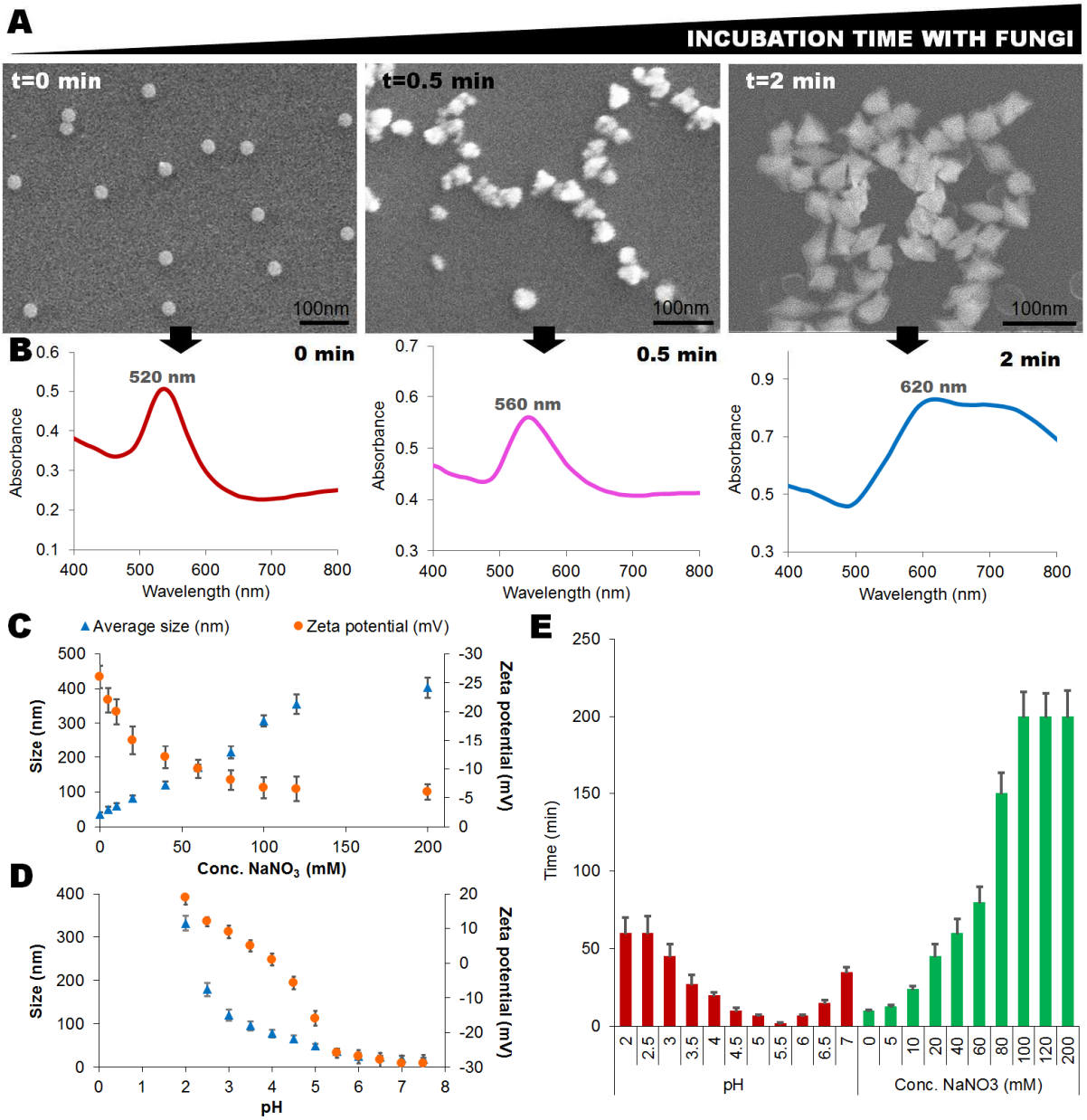

Figure 2. Surface plasmon resonance and stability assays of gold nanoparticles after incubation with *Aspergillus niger* and no *Aspergillus niger*.

(**A**) SEM images of the formation of gold nanoparticles, deposited on a silicon substrate. In the absence of *Aspergillus niger* fungi (t=0 min), the gold nanoparticles are seen to be spherical shaped under SEM. After 30 seconds incubation with fungi, some aggregation is observed, and after 2 minutes, a change in shape to nanostar like particles is observed. (**B**) Surface Plasmon Resonance spectra of nanoparticles with increasing incubation times is shown; red, nanospheres at (t=0), purple nano-aggregates at (t=0.5min) and blue, nanostars at (t=2min). (**C**) Gold nanoparticle formulation in the presence of $NaNO_3$. (**D**) Dependence of Gold nanoparticle formulation on pH value. (**E**)

Dependence of the duration of gold nanoparticle formulation time on pH (red) and $NaNO_3$ concentration (green) (N=6).

Table 1. Physico-chemical characteristics of Gold nanoparticles. (N=6)

Gold nanoparticle	Hydrodynamic Diameter (nm)	Zeta Potential (mv)	$\lambda_{max}\xi$ (nm)
Month 0	37.7±3.2	26.1±1.5	530±9
Month 1	35.5±3.3	25.2±1.8	529±11
Month 2	38.1±3.4	26.3±2.1	530±15
Month 3	34.7±3.1	25.7±1.9	528±17
Month 4	35.4±2.8	26.2±1.7	529±12
Month 5	37.2±3.0	25.9±1.5	530±17
Month 6	36.6±1.9	25.5±2.1	530±18

Characterization of Plasmonic Colloidal Gold diagnostic reagents present in the presence of *Aspergillus niger* cultures

When 100 µL of *Aspergillus niger* at a concentration of 100 CFU/mL were added to the 100 µL of Chloroauric acid and HEPES buffer, the particles began to form aggregates and the spherical shape became distorted on the silicon wafer substrate (Figure 2A, t=0.5 mins). This is consistent with the observed dramatic change in the positioning of the surface plasmon resonance, which now exhibits a maximum at a wavelength of 560 nm. When the incubation time is increased to 2 mins, the nanoparticles precipitated onto the silicon substrate develop distinct pointed features and have dimensions of ~35 nm (Figure 2A, t=2 mins), a form which is commonly referred to as “nanostars”. They are characterised by a doubly peaked Surface Plasmon Resonance spectrum, with maxima at wavelengths of 620 nm and 720 nm. The change in the surface plasmon resonance peak from 520 to 620/720 nm corresponds to a striking, visible colour change from orange/red to blue (Figure 2B).

The formation processes can be visualised by monitoring the absorbance ratio 520nm/620nm, as shown in Fig. S4 (see Electronic Supplementary Material, ESM). For the case of 100 µL of *Aspergillus niger* at a concentration of 100 CFU/mL and a pH of 5.5., this ratio is seen to stabilise at a value of 0.8 after 2 minutes. This point of stabilisation can be used as a characteristic formation time, and Figure 2E demonstrates that, as a function of pH, this formation time is strongly pH dependent. In the presence of 16 CFU/ml *Aspergillus niger*, when the pH value of the Chloroauric

acid and HEPES buffer suspension is below 5.0, DLS measurements indicate that the size of gold nanoparticle increases. The Zeta potential changed from 26mV at pH 5.5 to 16 mV at pH 5. This result is consistent with literature results on the relationship of gold nanoparticle size with pH value and Zeta potential [30, 31]. UV/

Notably, there is a lowest time point at pH 5.5 for the duration of gold nanoparticle formulation. The colour is easily identified and distinguishable with the naked eye, as it turns a blue in colour within 2 min. The duration is optimized to produce a rapid test in 2 mins. The pH is set at 5.5 in the following experiment for fungi detection.

The aggregation process can also be induced by 5 mM $NaNO_3$ (Figure 2E). DLS measurements show an increase in the average particle size from 35.0 ±5.6 to 402±29 nm as $NaNO_3$ concentration is increased from 0-200 mM. The Zeta potential changes from 26mV to 6 mV when $NaNO_3$ concentration is increased over the same range. Notably, however, the gold nanoparticle formulation time also increases significantly. When the $NaNO_3$ concentration is equal to 0, the particle formulation takes 10 mins (Figure 2E). When the $NaNO_3$ concentration is increased, it takes over 200 mins to form large nanoparticles (400 nm in diameter, see Figure 2E and ESM Fig. S5). The salt-induced aggregation arises due to shielding of the electrostatic repulsion between the negatively charged nanoconjugate systems. The electrostatic repulsion is mediated by formation of an electrical double layer to form a large nanoparticle [30, 31]. The colour of the solution appears grey or transparent due to large nanoparticle formulation [20].

The images of living fungi typically exhibit many long hyphae connected on the core of *Aspergillus niger*. Gold nanoparticles are deposited on the glass substrate or trapped between hyphae (Figure 3B-D). Some gold nanoparticles have been found also on the fungi hypha mixing fungi with Chloroauric acid and HEPES buffer after 2 minutes of incubation (Figures 3A). An enlargement of the rectangular area shows star shaped gold nanoparticle on of the fungi hyphae (Figure 3A**)**. The right side of the panel shows the rectangular area of the left panel of Figure 3A.

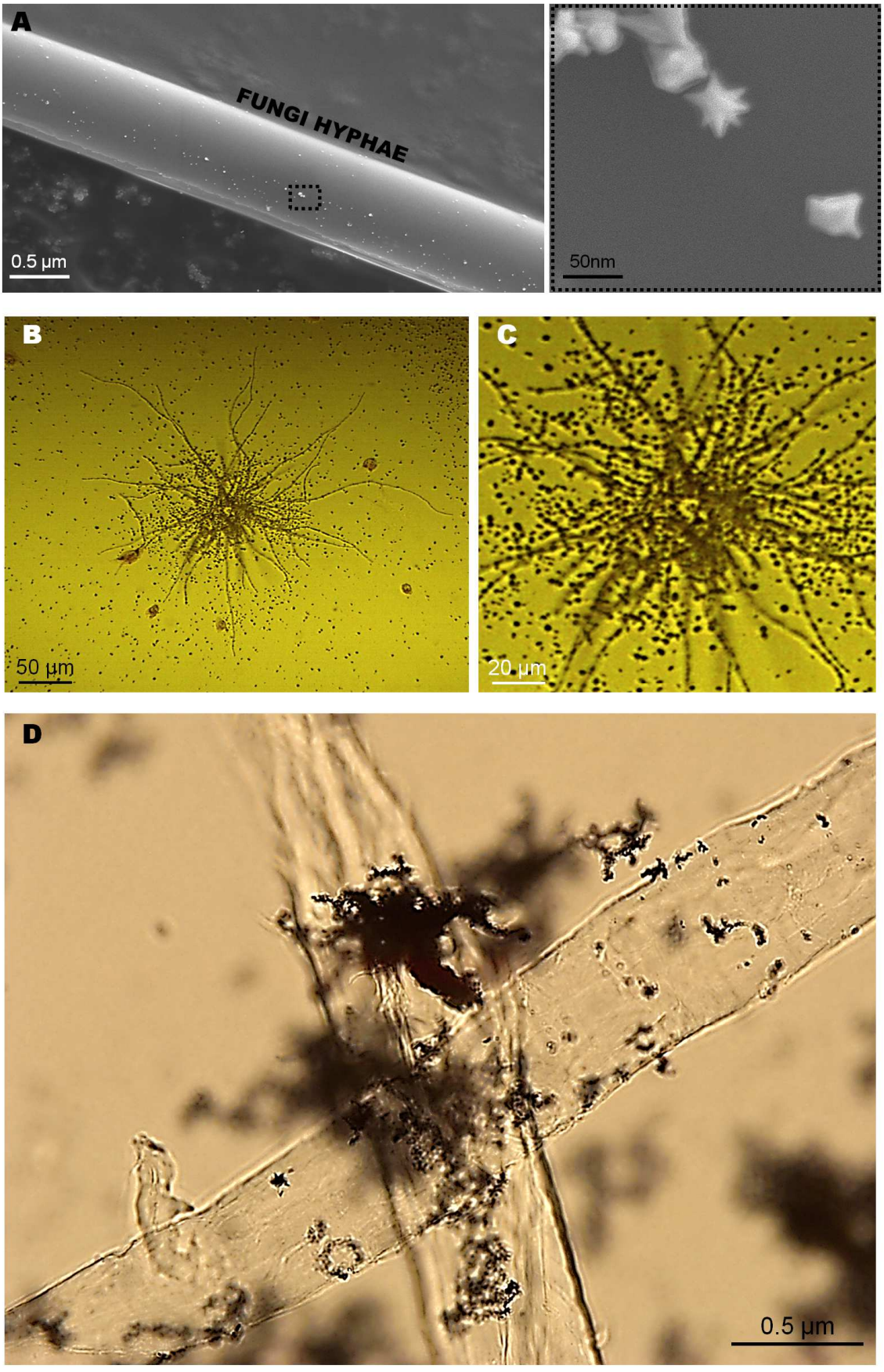
A
FUNGI HYPHAE
0.5 µm
50nm
B
50 µm
C
20 µm
D
0.5 µm

Figure 3. (**A**) SEM images of hyphae of *Aspergillus niger* growing in gold nanoparticle solution after 2 minutes of incubation. The right side of the panel shows the nanoparticles' morphology on the hyphae of *Aspergillus niger*. Images of *Aspergillus niger* and gold nanoparticles under light microscopy, under a 4× microscope objective, (B) 10× microscope objective and (C) 100× microscope objective (D). The images of living fungi typically exhibit several long hyphae connected on the core of fungi (B, C).

Generation of coloured solutions for *Aspergillus niger* detection with the naked eye

A change in colour from red to blue was detected in a number of human samples, indicating the presence of fungal infection. The efficiency of the colloidal gold diagnostic reagent in detecting *Aspergillus niger* contamination is 100% in comparison to microscopy observation. A blue colour indicated fungi contamination (from top second to third line in the of the 96-well plate image in Figure 4A). Detection with the naked eye seems perfectly suited for analyses in laboratories or public places with fewer resources. The colour changed from bright red to blue (indicating the nano star formation) in 120 seconds. These results show that the red colour is directly attributable to the sphere shaped gold nanoparticles, whereas, when in contact with the *Aspergillus niger*, the spherical shaped nanoparticles change to star shaped with a concomitant change in colour from red to blue. Therefore, it is deemed possible to measure fungi contamination by controlling the colour of the nanoparticle solution from red to blue (Figure 4A and 4B).

Notably, *Escherichia coli*, *Bacillus cereus* and *Staphylococcus aureus* show different colour changes at the same concentration and same bacterial concentration (S2). Bacterial experiments have the same order as fungi in 96 well plates and use same concentration as in the fungi experiments, from 0 CFU to 16 CFU/mL. The colour of the solution in bacteria samples changes from pale yellow to pink in 50 mins, at the same concentration as that of the fungi experiment (see ESM, Fig. S2). Since the difference in biomass of fungi and bacteria is large, it is difficult to compare the bacteria and fungi mechanism of gold nanoparticle formulation [38,39]. Particularly at low pH, biosorption on fungal biomass is higher than on bacteria [40, 41].

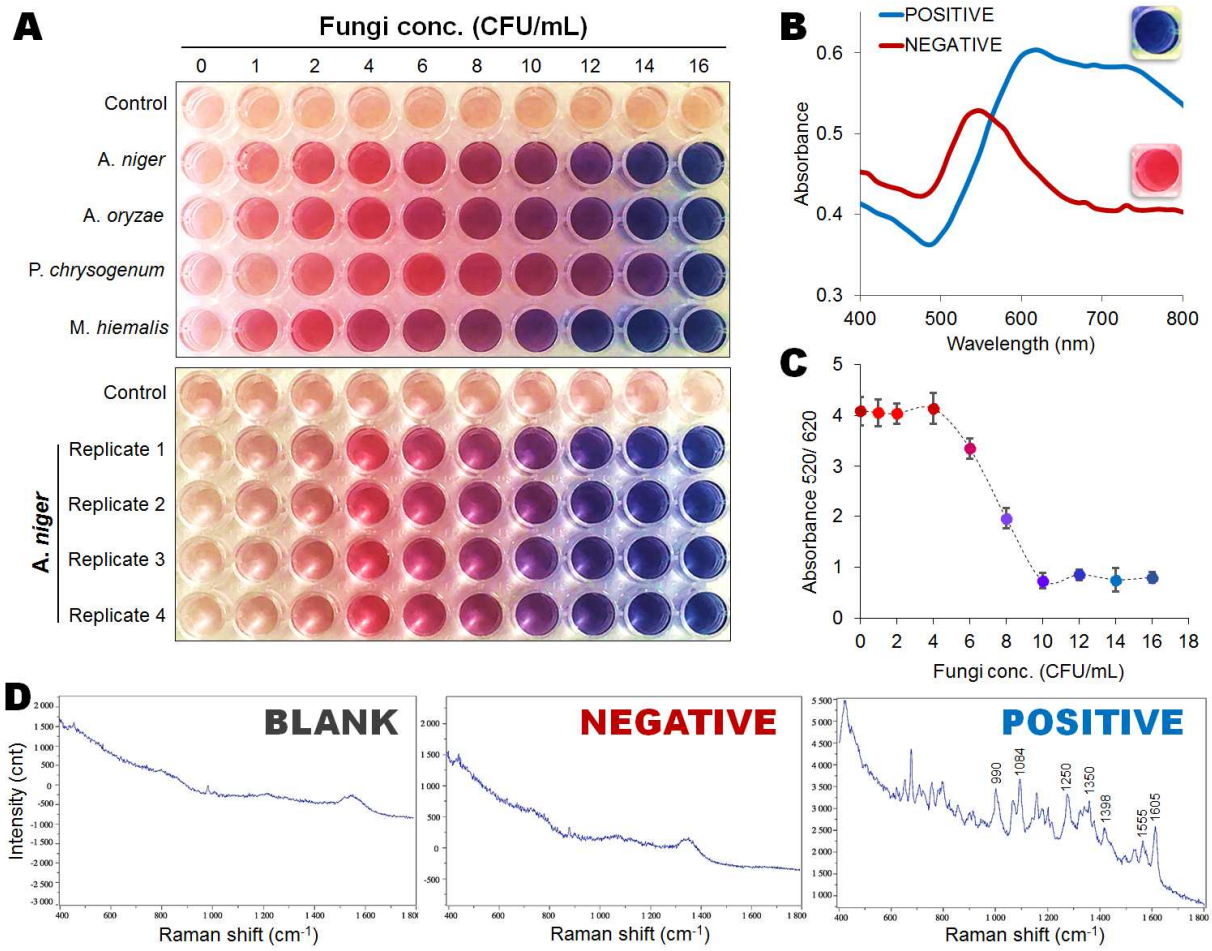

Figure 4. The correlation between colorimetric, surface plasmon resonance and Raman spectroscopy of Plasmonic fungi Gold nanoparticle. (**A**) Colorimetric assay of Gold nanoparticle in 96 well plate. (Upper panel) The concentration of *fungi* increases from left to right from 0 to 16 CFU/mL. And *Aspergillus niger*, *Aspergillus oryzae*, *Penicillium chrysogenum* and *Mucor hiemalis* were loaded from top to bottom, respectively. (Lower panel) The concentration of *Aspergillus niger* increases from left to right from 0 to 16 CFU/mL and the wells from 2nd row to 5th row are replicates. The colour changes from red to pink-purple and to blue indicated the increase in fungi concentration. (**B**) The surface plasmon resonance spectra under spectrometer reader of negative and positive samples for fungal infection. The negative one shows red colour and the positive shows blue colour. (**C**) Ratio between non-aggregated/negative sample (at 520 nm) and aggregated/positive GNPs (at 620 nm). The ratio of absorbances exhibits a plateau below ~ 4 CFU/mL, and above 10 CFU/mL, which define the limits of detectability, which an approximately linear region in between. (**D**) Raman spectra of a Blank, Negative and Positive samples. No Raman spectra is present in the Blank and Negative samples; however an intensive Raman spectra can be observed in Positive samples.

The change in colour was correlated with a change in the surface plasmon resonance peak. The surface plasmon resonance peak of the solution without fungi occurs at 520 nm, whereas in the solution with fungi the peak was shifted to higher wavelengths (i.e. 620 nm) (Figure 4B). Therefore, the absorbance ratio between non-aggregated/negative sample (at 520 nm) and aggregated stars/positive GNPs (at 620 nm) are correlated with the colour change. In order to find the relationship between concentration of fungi and colour density, the ratio of absorbance at 520 nm/ 620 nm was again employed as an indicator of the process. The ratios of absorbance at the two wavelengths were calculated and the mean values were plotted as a function of concentration of fungi. When the concentration varies from 4-10 CFU/mL, the colour appears 'purple'. When the concentration is higher than 10 CFU/mL, the colour appears blue. The ratio of absorbances exhibits a plateau below ~ 4 CFU/mL, and above 10 CFU/mL, which define the limits of detectability, with an approximately linear region in between (Figure 4C). These results were also corroborated by Raman spectroscopy. Figure 4D depicts the Raman spectra of Blank, Negative and Positive samples. No Raman spectra can be found in blank and negative samples, whereas in the positive sample characteristic peaks and high intensity Raman shifts can be observed (Figure 4D), indicating SERS of *Aspergillus niger* contamination. The coherence of colour changes, surface plasmon resonance and Raman spectra confirm the robustness of the gold nanoparticle for detection of fungal infections. The Raman features in the region of 990 cm^{-1} and at 1084 cm^{-1} correspond to P=O symmetric and P=O symmetric stretching, respectively, and indicate the presence of protein phosphate groups. Two bands are seen at 1250 and 1350 cm^{-1}. These bands may be assigned to the amide II bands of proteins. The intense bands at 1555 and 1605 cm^{-1}, correspond to aromatic skeletal vibration plus C=C stretching (amide I and II bands). The peak at 1398 cm^{-1} is assigned to the COO^- symmetric stretch from proteins with carboxyl side groups in the amino acid residues. The presence of amide linkages suggests that there are some proteins in the reaction mixture from fungi [30, 42, 43]. These proteins may play an important role in the morphological transformation of nanoparticles [44, 45].

Comparison of four fungi on gold nano particle formulation

Table 2. Physico-chemical characteristics of gold nanoparticles mixing different fungi (N=4)

Samples	Hydrodynamic Diameter (nm)	Zeta Potential (mV)	λ_{max} (nm)
Aspergillus *niger*	40±9.2	7.5±0.4	560±8
Aspergillus *oryzae*	38±7.1	7.8±0.2	560±12
Penicillium *chrysogenum*	40±13	11.6±1.9	563±12
Mucor *hiemalis*	51±11	9.6±3.6	565±15

Hydrodynamic diameters of gold nanoparticles were measured from mixing different fungi at a concentration of 16 CFU/ml with Chloroauric acid and HEPES buffer after 2 minutes of incubation. The average sizes range from 38±7.1 nm to 51±11 nm. The zeta potential of four types of gold nanoparticles is around 7.5 mV to 11.6 mV. The peaks of surface plasma resonance are from 560 nm to 565 nm. Bhambure and co-authors have employed *Aspergillus niger* with uric chloride to produce gold nanoparticles at diameter of 12.79 nm [42]. The particle formulation is related with pH value [30, 31]. The *Aspergillus niger* had a rather narrow pH optimum around pH 5.5 to active phytase [46]. In this experiment, a pH value equal to 5.5 is optimized to shorten the synthesis time and aimed a rapid colour changing.

Since A.niger and *A.oryzae* are all aspergillus, the colour changes observed are the same (see ESM, Fig. S1). The wells of 4th row are *P. chrysogenum* and 5th rows are *M. hiemalis* (Figure 4A). Different fungi have different impact on the gold nanoparticle formulation. The composition of protein phosphate groups and amino acid are large different on fungi. *Aspergillus fumigatus*, *Emericella nidulans,* and *Myceliophthora thermophile* phytases exhibited considerable activity with a broad range of phosphate compounds. It has been considered that more phosphate is liberated by the *A. fumigatus* phytase than by the *A. niger* phytase [46]. The different enzyme activity from different fungi cause gold nanoparticle formulation slight different, but all of fungi, such as *A.niger* , *A.oryzae* and *M.hiemalis*, are able to detect at the concentration of 10 CFU/mL.

Comparison between Gold nanoparticle and KOH on Athlete's foot from human patients

The current gold standard for the screening of superficial fungal infections is the KOH test. The infected sample incubated with potassium hydroxide can be observed under a fluorescence microscope.

Standard fungi cultures with agar plates are accurate but can take up to seven days to positively identify the contaminating fungus. The diagnosis of infection versus colonization with these fungi is time consuming. The agar plate incubation is slow and expensive, but useful to confirm the diagnosis of onychomycosis when long-term oral therapy is being considered. The culture usually takes 5 days to be declared positive; it must be held for 21 days until being declared negative. If fungal infections are mistreated as other diseases, the different drugs used may cause fungal resistance and will challenge the treatment. ELISA and Real-time PCR are much faster but require expensive equipment and reagents [19].

Notably, the GNPs method is much simpler and faster, and most importantly revealed no statistical difference between this method and the existing KOH method (Table 3). In fact, specificity and sensitivity of GNPs have been evaluated against the existing clinic method, KOH, on the same samples. The KOH test has 71.3% sensitivity and a 94.4% specificity for the diagnosis of Athlete's foot, compared with an 80 % sensitivity and 95% specificity for gold nanoparticle method (Table 3). The negative predictive value (NPV) is the percentage of patients with a negative test who do not have the disease. In 2×2 table (Table 3), Cell "d" are the "True Negatives" and Cell "c" are the "False Negatives". NPV tells us how many of the test negatives true negatives are; and if this number is 90%, then it suggests that this new test is doing as well as the "Gold Standard". Moreover, the GNPs (200 µl per test) represent a dramatic reduction in the cost of generating results, and the GNPs delivers precise results of fungi detection after 2 minutes of incubation only.

Furthermore, the GNP method offers incubation free and storage at room temperature, eliminating the need for an incubator and refrigeration space. It requires low cost and no complex equipment to achieve precise results. The main factor of this test is the fact that detection of a microbial contaminant can be made with the naked eye, perfectly suited for analyses in laboratories, public places or farms/livestock infrastructures with fewer resources in only 2 minutes. The small sample size has been tested on both methods. The predictions give means the KOH method can successfully predict the outcome (p value =0.0022). The predictions give means the gold nanoparticle method can more successfully predict the outcome (p value =0.0019).

Table 3 Comparison between Gold nanoparticle test and KOH on Athlete's foot from human patients.

Two-tail analysis with Fisher's test
KOH method

5 (a)	1(b)
2 (c)	17 (d)

P value =0.0022
The predictions given means the method can successfully predict the outcome.

Gold nanoparticle method

4 (a)	1(b)
1 (c)	19 (d)

Exact p-value=0.0019

The predictions given means the method can successfully predict the outcome.

	KOH		Nanoparticles	
Statistic	Value	95% CL	Value	95% CL
Sensitivity	71.4%	29.0 % to 96.3 %	80%	28.2 % to 99.5 %
Specificity	94.4 %	72.7 % to 99.9 %	95%	75.1 % to 99.9 %
Positive Predictive Value (PPV)	83.3%	41.3 % to 97.3 %	80%	36.0% to 96.6 %
Negative Predictive Value (NPV)	89.5 %	72.4 % to 96.5 %	95%	76.7 % to 99.1 %

It is known that microorganisms such as bacteria [39] and fungus [40] are capable of producing gold nanoparticles from solutions containing ionic gold. Notably, while the time required for the process in the presence of bacteria ranges from 24 to 48 h [39]. The mechanism of gold nanoparticles formation in the presence of fungi/bacteria is still not well known, however. Raman spectroscopy shows there are phosphate, aromatic and carboxyl side groups in amino acid residues in the reaction mixture of fungi, consistent with literature [30,45,46]. These amino acid residues may play an important role in the formation and morphological transformation of nanoparticles [47,48].

The differing spectral evolution patterns for fungal pathogens compared to bacteria and other factors such as salt concentrations, render the test specific to such infections. Table 3 demonstrates that the test is comparable in terms of specificity to the KOH test, but has the advantage of being significantly more rapid and convenient. Neither the KOH test nor the GNPs method allows specific identification of a specific fungal pathogen. Further microbiological testing must be performed to permit identification of a specific pathogen. However, the knowledge can be transferable and applicable to other health problems related to fungal infections as well. The system described here has been initially developed, tested and implemented for athlete's foot. The sensitivity (10 CFU/ml) achieved with the GNPs is not only sufficient to diagnose athlete's foot in order to target bathing water regulations, but can also provide information on waterborne disease outbreaks [47,48].

Aspergillus fumigatus, *Emericella nidulans*, and *Myceliophthora thermophile* phytases exhibited considerable activity with a broad range of phosphate compounds. The *Aspergillus niger* had a rather narrow pH optimum around pH 5.5 to active phytase [46]. However, the knowledge of the interaction between fungal enzyme activities with gold nanoparticle is still at an early stage. The large and relatively unexplored fungal enzyme activity is an advantage because of the role that extracellular proteins and enzymes have in Au reduction and GNP capping. We plan to implement a systematic study such as protein phosphate groups and amino acid on mechanism of fungi on colour changing of gold nanoparticles in the near future.

CONCLUSIONS

A novel Gold nanoparticle based, rapid detection system has been developed to diagnose fungi infection in a fast and simple way. The correlation of the colour change (absorbance of 520nm/620nm) is related to fungi concentration. The cut of ration is 0.8 on 520nm/620 nm. There was a significant colour change from red to blue when the fungi concentration increased from 0 to 16 CFU/mL. When the fungi concentration at 10 CFU/mL, the ration of 520nm/620nm was significant decrease. When the bacterial concentration increase, the ration of 520nm/620nm was slowly decrease. There is a linear relationship between concentration of *E.coli* and the ration from 0-16 CFU/mL with a low slope on the curve. The resolution of this test was 10 CFU/mL. The current gold standard KOH was compared with the GNP method for the diagnosis of fungal infection. The GNP method has an 80% sensitivity and a 95% negative predictive value for the diagnosis of athlete's foot

from human donors. We found no statistical difference between our method and the gold standard method KOH. The gold nanoparticles application has an outstanding potential to contribute for surface hygiene at home or public places simply by monitoring a colour change with naked eye.
This approach requires no extraneous instrumentation or prior sample preparation and has a rapid and simple diagnostic readout that could be used in clinical settings for testing patient samples or in field tests to monitor food and water sources.

ACKNOWLEDGMENTS

Tobiloba Sojinrin and Kangze Liu thanks Fiosraigh Scholarship Programme from Dublin Institute Technology. Furong Tian acknowledges Enterprise Ireland CF-2015-0269-Y. This work is supported by National Natural Scientific Fund (No.81225010), 863 Project of China (2014AA020700), Shanghai Science and Technology Fund (No.13NM1401500), Shanghai Jiao Tong University Innovation Fund for Postgraduates (No. AE340011).

AUTHOR CONTRIBUTIONS

Conceived and designed the experiments: Tobiloba Sojinrin, João Conde, Kangze Liu, James Curtin, Furong Tian. Analysed the data: Tobiloba Sojinrin, João Conde, Kangze Liu, Furong Tian. Contributed reagents/materials/analysis tools: James Curtin, Daxiang Cui, Furong Tian. Wrote the paper: Kangze Liu, James Curtin, Hugh J Byrne, Furong Tian, Tobiloba Sojinrin.

ETHICAL COMMITTEE APPROVAL

Clinical specimen experiments were performed according to Guidelines for Ethical Committee, Shanghai Jiao Tong University. All the experiments used in this study were complied with current ethical considerations: Approval (SYXK-2007-0025) of Ethical Committee of Shanghai Jiao Tong University (Shanghai, China).

DECLARATION ON CONFLICT OF INTEREST

The Authors declare that there is no conflict of interest.

REFERENCES

1. Free TA (2002) Current Diagnosis and Treatment in Infectious Diseases. The Nurse Practitioner 27 (2):43
2. Kirk P, Cannon P, David J, Stalpers J (2001) Ainsworth and Bisby's dictionary of the fungi. Ainsworth and Bisby's dictionary of the fungi: 9th edition (Ed. 9)
3. Fleming RV, Walsh TJ, Anaissie EJ (2002) Emerging and less common fungal pathogens. Infectious disease clinics of North America 16 (4):915-933
4. McNeil MM, Nash SL, Hajjeh RA, Phelan MA, Conn LA, Plikaytis BD, Warnock DW (2001) Trends in mortality due to invasive mycotic diseases in the United States, 1980–1997. Clinical Infectious Diseases 33 (5):641-647
5. Elewski BE (1998) Onychomycosis: pathogenesis, diagnosis, and management. Clinical microbiology reviews 11 (3):415-429
6. Vélez A, Linares MJ, Fenández-Roldán JC, Casal M (1997) Study of onychomycosis in Cordoba, Spain: prevailing fungi and pattern of infection. Mycopathologia 137 (1):1-8
7. Godoy P, Nunes F, Silva V, Tomimori-Yamashita J, Zaror L, Fischman O (2004) Onychomycosis caused by Fusarium solani and Fusarium oxysporum in Sao Paulo, Brazil. Mycopathologia 157 (3):287-290
8. Kemna ME, Elewski BE (1996) A US epidemiologic survey of superficial fungal diseases. Journal of the American Academy of Dermatology 35 (4):539-542
9. Sellami A, Sellami H, Makni F, Mezghani S, Cheikh-Rouhou F, Marrekchi S, Turki H, Ayadi A (2008) Childhood dermatomycoses study in Sfax hospital, Tunisia. Mycoses 51 (5):451-454
10. Svejgaard E, Nilsson J (2004) Onychomycosis in Denmark: prevalence of fungal nail infection in general practice. Mycoses 47 (3-4):131-135
11. Baran R (2011) The nail in the elderly. Clinics in dermatology 29 (1):54-60
12. Baran R, Haneke E, Hay RJ, Piraccini BM, Tosti A (1999) Onychomycosis: the current approach to diagnosis and therapy. CRC Press,
13. Bontems O, Hauser P, Monod M (2009) Evaluation of a polymerase chain reaction□restriction fragment length polymorphism assay for dermatophyte and nondermatophyte identification in onychomycosis. British Journal of Dermatology 161 (4):791-796
14. Kitching M, Ramani M, Marsili E (2015) Fungal biosynthesis of gold nanoparticles: mechanism and scale up. Microbial biotechnology 8 (6):904-917
15. Han HW, Hsu MM-L, Choi JS, Hsu C-K, Hsieh HY, Li HC, Chang HC, Chang TC (2014) Rapid detection of dermatophytes and Candida albicans in onychomycosis specimens by an oligonucleotide array. BMC infectious diseases 14 (1):1
16. Pickering JW, Sant HW, Bowles CA, Roberts WL, Woods GL (2005) Evaluation of a (1→ 3)-β-d-glucan assay for diagnosis of invasive fungal infections. Journal of Clinical Microbiology 43 (12):5957-5962
17. Van Thiel DH, George M, Moore CM (2012) Fungal infections: their diagnosis and treatment in transplant recipients. International journal of hepatology 2012
18. Guarner J, Brandt ME (2011) Histopathologic diagnosis of fungal infections in the 21st century. Clin Microbiol Rev 24 (2):247-280. doi:10.1128/CMR.00053-10
19. Andrews MD, Burns M (2008) Common tinea infections in children. Am Fam Physician 77 (10):1415-1420
20. Sugunan A, Melin P, Schnurer J, Hilborn JG, Dutta J (2007) Nutrition-driven assembly of colloidal nanoparticles: growing fungi assemble gold nanoparticles as microwires. Advanced Materials 19 (1):77-81

21. Li Z, Chung SW, Nam JM, Ginger DS, Mirkin CA (2003) Living templates for the hierarchical assembly of gold nanoparticles. Angew Chem Int Ed Engl 42 (20):2306-2309. doi:10.1002/anie.200351231
22. Conde J, Bao C, Cui D, Baptista PV, Tian F (2014) Antibody-drug gold nanoantennas with Raman spectroscopic fingerprints for in vivo tumour theranostics. J Control Release 183:87-93. doi:10.1016/j.jconrel.2014.03.045
23. Bao C, Chen L, Wang T, Lei C, Tian F, Cui D, Zhou Y (2013) One Step Quick Detection of Cancer Cell Surface Marker by Integrated NiFe-based Magnetic Biosensing Cell Cultural Chip. Nano-Micro Letters 5 (3):213-222
24. Conde J, Tian F, Hernandez Y, Bao C, Cui D, Janssen KP, Ibarra MR, Baptista PV, Stoeger T, de la Fuente JM (2013) In vivo tumor targeting via nanoparticle-mediated therapeutic siRNA coupled to inflammatory response in lung cancer mouse models. Biomaterials 34 (31):7744-7753. doi:10.1016/j.biomaterials.2013.06.041
25. Conde J, Ambrosone A, Sanz V, Hernandez Y, Marchesano V, Tian F, Child H, Berry CC, Ibarra MR, Baptista PV, Tortiglione C, de la Fuente JM (2012) Design of multifunctional gold nanoparticles for in vitro and in vivo gene silencing. ACS Nano 6 (9):8316-8324. doi:10.1021/nn3030223
26. Bao C, Beziere N, del Pino P, Pelaz B, Estrada G, Tian F, Ntziachristos V, de la Fuente JM, Cui D (2013) Gold nanoprisms as optoacoustic signal nanoamplifiers for in vivo bioimaging of gastrointestinal cancers. Small 9 (1):68-74
27. Bhaskar S, Tian F, Stoeger T, Kreyling W, de la Fuente JM, Grazu V, Borm P, Estrada G, Ntziachristos V, Razansky D (2010) Multifunctional Nanocarriers for diagnostics, drug delivery and targeted treatment across blood-brain barrier: perspectives on tracking and neuroimaging. Part Fibre Toxicol 7:3. doi:10.1186/1743-8977-7-3
28. Bao C, Tian F, Estrada G (2011) Improved visualisation of internalised carbon nanotubes by maximising cell spreading on nanostructured substrates. Nano Biomedicine and Engineering 2 (4):201-210
29. De La Rica R, Stevens MM (2012) Plasmonic ELISA for the ultrasensitive detection of disease biomarkers with the naked eye. Nature nanotechnology 7 (12):821-824
30. Das SK, Dickinson C, Lafir F, Brougham DF, Marsili E (2012) Synthesis, characterization and catalytic activity of gold nanoparticles biosynthesized with Rhizopus oryzae protein extract. Green Chemistry 14 (5):1322-1334
31. Tian F, Bonnier F, Casey A, Shanahan AE, Byrne HJ (2014) Surface enhanced Raman scattering with gold nanoparticles: effect of particle shape. Analytical Methods 6 (22):9116-9123
32. Mukherjee P, Senapati S, Mandal D, Ahmad A, Khan MI, Kumar R, Sastry M (2002) Extracellular synthesis of gold nanoparticles by the fungus Fusarium oxysporum. Chembiochem 3 (5):461-463. doi:10.1002/1439-7633(20020503)3:5<461::AID-CBIC461>3.0.CO;2-X
33. Cohen R, Persky L, Hadar Y (2002) Biotechnological applications and potential of wood-degrading mushrooms of the genus Pleurotus. Applied Microbiology and Biotechnology 58 (5):582-594
34. Fischbach FT, Dunning MB (2009) A manual of laboratory and diagnostic tests. Lippincott Williams & Wilkins,
35. Tian F, Conde J, Bao C, Chen Y, Curtin J, Cui D (2016) Gold nanostars for efficient in vitro and in vivo real-time SERS detection and drug delivery via plasmonic-tunable Raman/FTIR imaging. Biomaterials 106:87-97.

36. Singh DK, Ganbold E-O, Cho E-M, Cho K-H, Kim D, Choo J, Kim S, Lee CM, Yang SI, Joo S-W (2014) Detection of the mycotoxin citrinin using silver substrates and Raman spectroscopy. Journal of hazardous materials 265:89-95
37. Khoury CG, Vo-Dinh T (2008) Gold nanostars for surface-enhanced Raman scattering: synthesis, characterization and optimization. The Journal of Physical Chemistry C 112 (48):18849-18859
38. Kuyucak N, Volesky B (1988) Biosorbents for recovery of metals from industrial solutions. Biotechnology letters 10 (2):137-142
39. Tsuruta T (2004) Biosorption and recycling of gold using various microorganisms. The Journal of general and applied microbiology 50 (4):221-228
40. Taherzadeh MJ, Fox M, Hjorth H, Edebo L (2003) Production of mycelium biomass and ethanol from paper pulp sulfite liquor by Rhizopus oryzae. Bioresource technology 88 (3):167-177
41. Xu B, Jahic M, Blomsten G, Enfors S-O (1999) Glucose overflow metabolism and mixed-acid fermentation in aerobic large-scale fed-batch processes with Escherichia coli. Applied microbiology and biotechnology 51 (5):564-571
42. Bhambure R, Bule M, Shaligram N, Kamat M, Singhal R (2009) Extracellular biosynthesis of gold nanoparticles using Aspergillus niger–its characterization and stability. Chemical engineering & technology 32 (7):1036-1041
43. Binupriya A, Sathishkumar M, Vijayaraghavan K, Yun S-I (2010) Bioreduction of trivalent aurum to nano-crystalline gold particles by active and inactive cells and cell-free extract of Aspergillus oryzae var. viridis. Journal of hazardous materials 177 (1):539-545
44. Gole A, Dash C, Ramakrishnan V, Sainkar S, Mandale A, Rao M, Sastry M (2001) Pepsin-gold colloid conjugates: preparation, characterization, and enzymatic activity. Langmuir 17 (5):1674-1679
45. Vigneshwaran N, Kathe AA, Varadarajan PV, Nachane RP, Balasubramanya RH (2007) Silver-protein (core-shell) nanoparticle production using spent mushroom substrate. Langmuir 23 (13):7113-7117
46. Wyss M, Brugger R, Kronenberger A, Rémy R, Fimbel R, Oesterhelt G, Lehmann M, van Loon AP (1999) Biochemical characterization of fungal phytases (myo-inositol hexakisphosphate phosphohydrolases): catalytic properties. Applied and environmental microbiology 65 (2):367-373
47. European Union (Drinking Water) Regulations (2014). S.I. No. 122/2014. Irish Statute Book, Ireland
48. Bathing Water Quality Regulations (2008). S.I. No. 79/2008. Irish Statute Book, Ireland

Analytical and Bioanalytical Chemistry

Electronic Supplementary Information

Plasmonic gold nanoparticle for detection of fungi and human cutaneous fungal infections

Tobiloba Sojinrin, João Conde, Kangze Liu, James Curtin, Hugh J Byrne, Daxiang Cui, Furong Tian

Layout of concentration of fungi and bacteria on 96 well plates

The mixture with 2 mM Chloroauric acid (10 µl) and 2 µl HEPES buffer in 88 µl distilled water was added to the 96 well plate. The wells of the first row were blank, containing 100 µl Ultrapure deionized water. The wells from the second to fifth row were filled with 100 µl fungi suspensions. The concentration of fungi were 0, 1, 2, 4, 6, 8, 10, 12, 14, 16 CFU/ml from left to right in each row. Four replicates have been measured for each data point. A plate layout of four fungi from top to bottom was comprised of *A. niger, A. oryzae*, *P. chrysogenum* and *M. hiemalis*. The wells from second to fifth row were replicas for each fungi 96-well plate (Fig. S1).

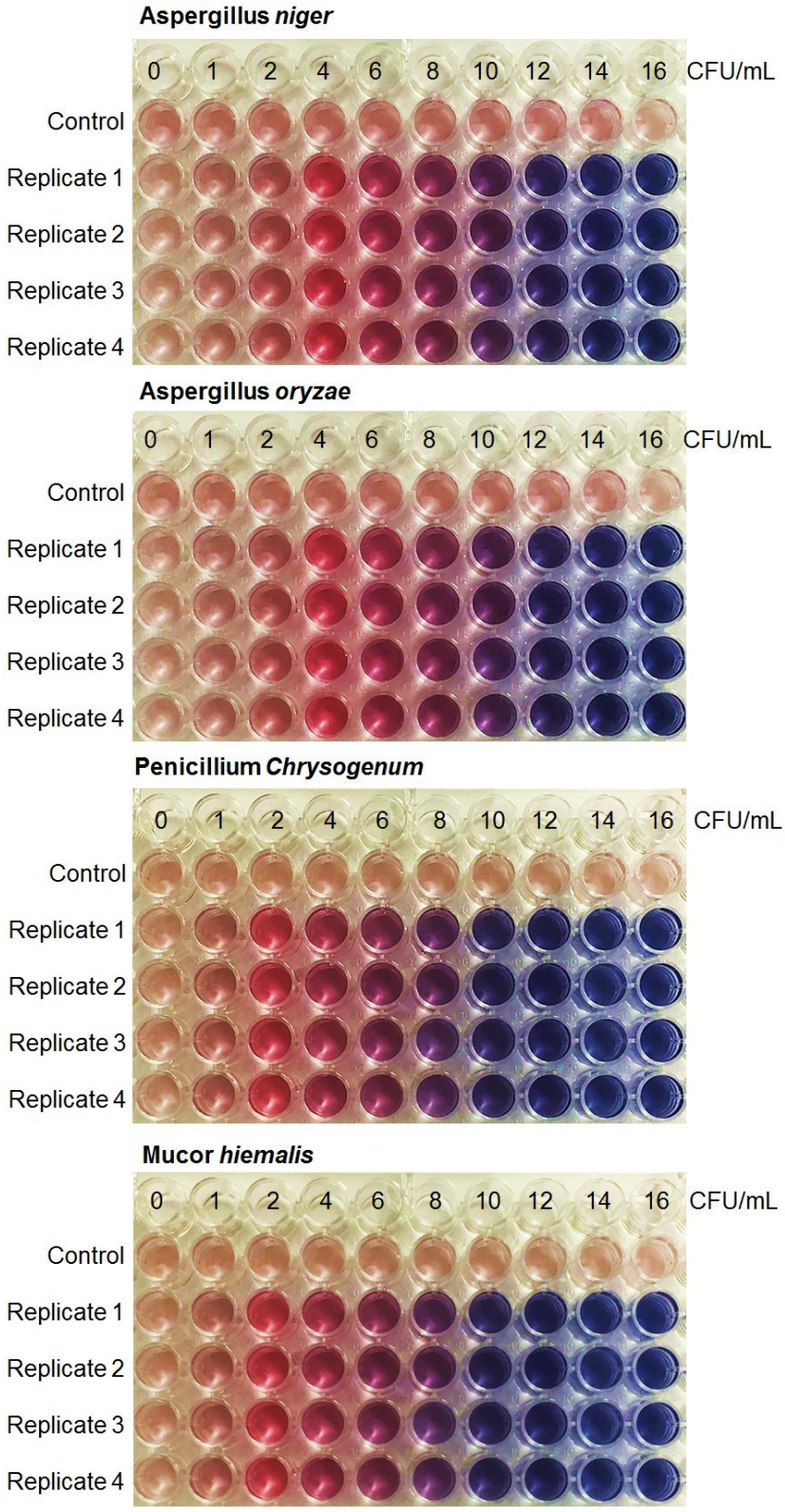

Fig. S1 Colorimetric assay of Gold nanoparticle on four different fungi in 96 well plate. The concentration of fungi increases from left to right from 0 to 16 CFU/mL and the wells from 2nd row to 5th row are replicates. The colour changes from red to pink-purple and to blue indicated the increase in fungi concentration

Layout of concentration of bacteria on 96 well plates

The mixture with 2 mM Chloroauric acid (10 µl) and 2 µl HEPES buffer in 88 µl distilled water was added to the 96 well plate. The wells of the first row were blank, containing 100 µl Ultrapure deionized water. The wells from the second to fifth row were filled with 100 µl bacteria suspensions. The plate layout of three bacterial samples starting from the second row to fourth row were *Escherichia coli*, *Bacillus cereus* and *Staphylococcus aureus* (Fig. S2).

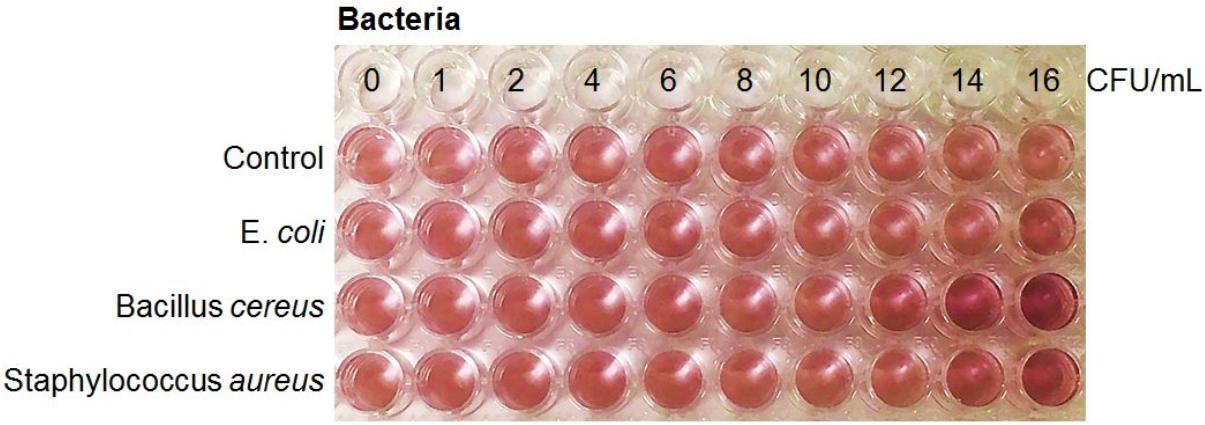

Fig S2 Colorimetric assay of Gold nanoparticle on three different bacteria in 96 well plate. The concentration of *bacteria* increases from left to right from 0 to 16 CFU/mL. *Escherichia coli*, *Bacillus cereus* and *Staphylococcus aureus* were loaded from top to bottom, respectively. The colour of the solution in bacteria samples changes from pale yellow to pink in 50 mins

Concentration depended Surface Plasma Resonance of gold nanoparticles on *Escherichia coli*

50 minutes after the addition of bacteria with HEPES buffer and $HAuCl_4$, a slow colour change was observed. When the bacterial concentration is increased over the range 0-16 CFU/mL, there is a minor shift of the SPR to higher wavelengths, with a slow decrease in the absorbance ratio concentration 520nm / 620nm. There is a linear relationship between concentrations of *Escherichia coli* and the ratio from 0-16 CFU/mL. The range of ratio observed was 2.3-1.6 at bacterial concentrations 0-16 CFU/mL (S3).

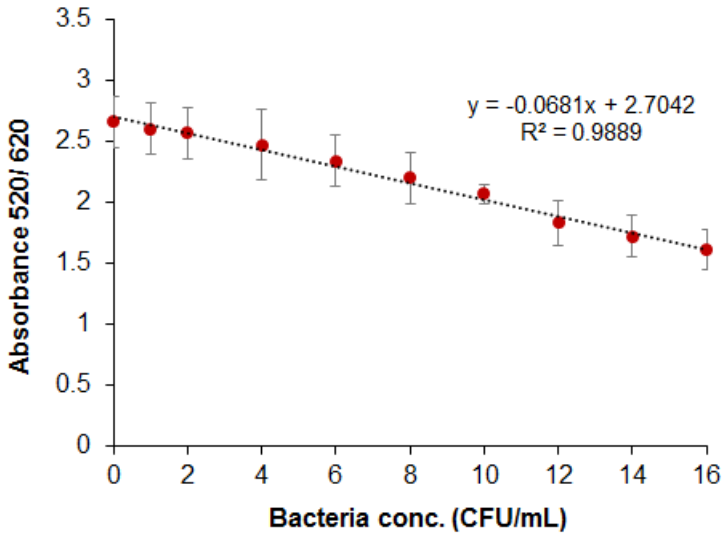

Fig. S3 SPR of gold nanoparticle formation and morphological transformation incubated with increasing concentrations of *Escherichia coli* at pH=5.5. Absorbance ratio 520nm/620nm following incubation of gold nanoparticles with increasing concentrations of *Escherichia coli*, in HEPES buffer

Time depended GNPs formation and morphological transformation on fungi and bacterial

With increasing time, a sharp and narrow SPR peak was observed at 530 nm within first 0.5 min of addition of fungi to $HAuCl_4$ with HEPES buffer in pH=5.5. Within 1 min, the absorption intensity of SPR peak was found to increase, and it was seen to red shift and broaden. This signifies polydispersity and increase in the size of synthesized GNPs within 2 mins. The ratio of absorbance 520 nm/620 nm was round to rapidly decrease from 4-0.8 in the time 0.5 min to 2 mins. At the time point of 2mins, the ratio stabilised at 0.8 (blue bars, Fig. S4), suggesting the completion of GNPS formation and morphological transformation.

In the case of bacteria, a modest and broad SPR peak was observed at 530 nm within the first 0.5 min of bacteria addition to $HAuCl_4$ with HEPES buffer. Within 2 min the absorption intensity of SPR peak was found to increase, at the same wavelength. The ratio of absorbance 520 nm/620 nm were increased slightly from 1.0-1.08 over the period from 0.5 min to 2 mins (red bars, Fig. S4). Bacteria can cause minor cause aggregation and red shifting of the SPR over a prolonged period of 50 mins (Fig. S3). This is a major drawback of procedures compared to fungi for rapid detection. Hence, the potential of this fungus towards such rapid GNP synthesis yielding a specific ratio of absorbance at 520 nm/620 nm at 0.8 presents a significant advantage in the context of a biosensor.

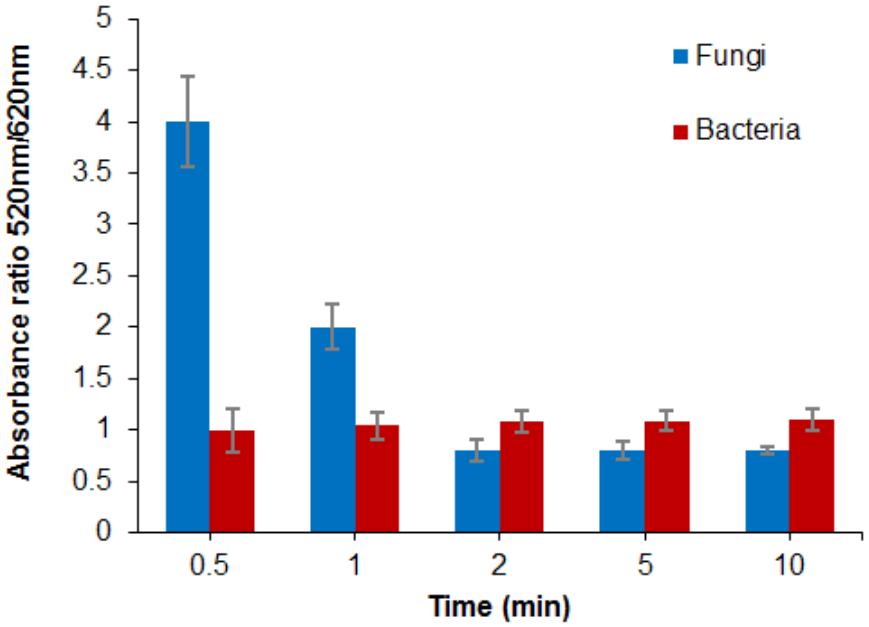

Fig. S4 Time dependent gold nanoparticle formation and morphological transformation on Bacteria (Red) and Fungi (Blue). The formation of gold nanoparticles over time was measured by the ratio of absorbance at 520nm/620nm from 0.5 min to 10 mins

Time depended Surface Plasma Resonance of GNPs on 200 mM of $NaNO_3$

In the presence of Na^+ alone, a different spectral evolution profile is observed, as shown in the typical time-course of GNP evolution in the presence of $NaNO_3$ (S5). The initial SPR resonance peak at ~530nm is slightly shifted and broadened over a period of ~50minutes and a broader resonance with maximum > 800nm evolves, associated with a colour change from pink to grey and transpired (Fig. S5).

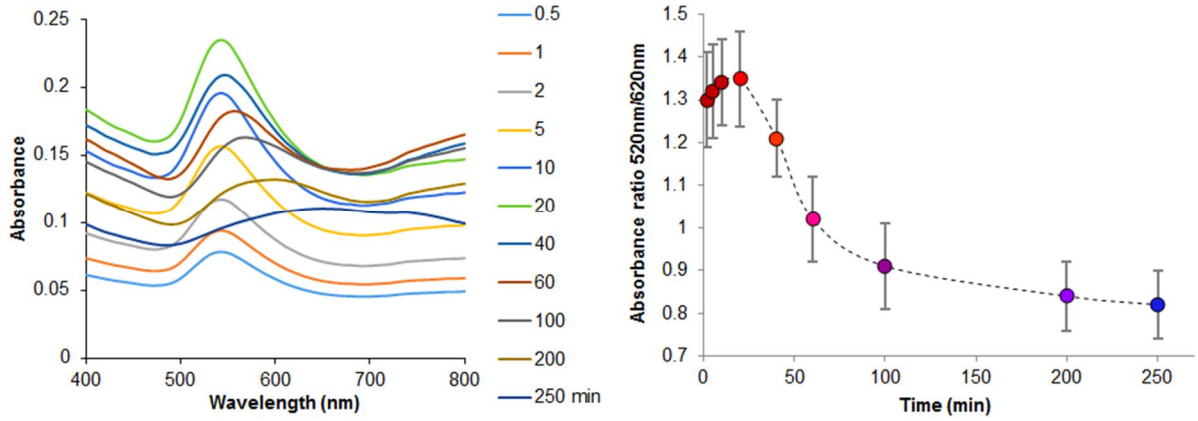

Fig. S5 Time dependent surface plasmon resonance (SPR) of gold nanoparticles formation and morphological transformation in sodium nitrate ($NaNO_3$). (Left panel) Absorbance spectra of nanoparticles after mixture with 200 mM of $NaNO_3$ in HEPES buffer at pH=5.5. The dotted lines shown the spectra of GNPs in 20 mins. (Right panel) The absorbance ratio 520 nm/620 nm gradually increased from 0.5 min to 20 mins, and slowly decreased at 40 min. At the time point of 200 mins, the ratio 520 nm/620 nm reached 0.8 (panel right)